2014

Influence of microstructural stability on the creep mechanism of Al-7wt% Si alloy processed by equal channel angular pressing

Materials Science & Engineering A 612 (2014) 162–171

Contents lists available at ScienceDirect

Materials Science & Engineering A

journal homepage: www.elsevier.com/locate/msea

Influence of microstructural stability on the creep mechanism of Al–7 wt% Si alloy processed by equal channel angular pressing

A. Orozco-Caballero [a,*], S.K. Menon [b], C.M. Cepeda-Jiménez [a,1], P. Hidalgo-Manrique [a,1], T.R. McNelley [b], O.A. Ruano [a], F. Carreño [a]

[a] Department of Physical Metallurgy, CENIM-CSIC, Avda. Gregorio del Amo 8, Madrid 28040, Spain
[b] Department of Mechanical and Aerospace Engineering, Naval Postgraduate School, Monterey, CA 93943-5146, USA

ARTICLE INFO

Article history:
Received 29 April 2014
Received in revised form
3 June 2014
Accepted 5 June 2014
Available online 14 June 2014

Keywords:
Al–Si alloys
Equal channel angular processing
Precipitate strengthening
Supersaturated solid solution
Deformation mechanism
Microstructural stability

ABSTRACT

A Na-modified, as-cast Al–7 wt% Si alloy was processed by equal channel angular pressing (ECAP) up to 8 passes by route A at ambient temperature using a 90° square section die, obtaining improved strength, ductility and work of fracture. From the first pass, porosity is removed, the eutectic constituent is refined and the eutectic silicon particles are partially redistributed. Additionally, a fine and homogeneous strain-induced silicon precipitation occurs in the supersaturated solid solution retained in the casting. These fine precipitates assist in grain refinement, resulting in a 250 nm grain size after one pass and 210 nm after 8 passes. This microstructure cannot sustain grain boundary sliding because it coarsens rapidly even at the lowest testing temperatures. Deformation at high temperatures gives values of n of about 8 and values of the activation energy corresponding to the self-diffusion of aluminum, 142 kJ/mol, which can be rationalized by a constant substructure slip creep mechanism. These values are influenced by the presence and evolution of the fine intradendritic silicon precipitates. Coarsening of these precipitates with time and temperature increases their interparticle distance causing variations in experimental n and Q values.

1. Introduction

Al–Si casting alloys are extensively used in the automotive and aerospace industries. This family of alloys has a wide range of possible industrial applications as a result of their low cost, good castability, moderate strength at room temperature and good wear resistance [1]. However, Al–Si casting alloys are poor in ductility and toughness. The influence of microstructural parameters such as dendrite size and Si particles shape and size have been studied extensively [2,3]. Many solutions have been proposed for controlling these parameters and improving the mechanical behavior, such as variations of solidification rates [4,5], additions of microstructure modifying elements [6], and performing various heat treatments [7].

Another approach to improve the mechanical properties of Al–Si casting alloys is to employ severe plastic deformation (SPD) which has been very effective in many alloy systems [8]. In the case of the Al–Si alloys different SPD techniques have been applied showing how microstructural homogenization and refinement lead to improvement of the mechanical properties [9,10]. Techniques such as friction stir processing may be applied to selected areas of a casting to achieve localized modification of microstructure and improvement of properties [11]. However, such a process involves a complex thermomechanical cycle. In contrast, equal channel angular pressing (ECAP) involves essentially isothermal deformation and a well-controlled strain history. This technique consists in pressing a billet through a die formed by the intersection of two channels. The billet cross section remains constant after one ECAP pass, and so the processing potentially can be repeated many times. ECAP processing has been widely applied to many metals and alloys, and the grain refinement obtained has been shown to increase the room temperature strength [12]. Nevertheless, not all the potential of ECAP processing has been revealed when applied to hypoeutectic Al–Si alloys.

The study of mechanical properties at intermediate to high temperatures has received little attention for these alloys. However, the beneficial microstructural changes produced by severe plastic deformation may improve considerably the creep resistance as observed in aluminum alloys [13,14] or may lead to superplastic behavior [15,16], which are of interest for high temperature applications or processing, respectively. Therefore,

* Corresponding author. Tel.: +34 91 5538900x217; fax: +34 91 5347425.
E-mail address: aorozco@cenim.csic.es (A. Orozco-Caballero).
[1] Present address: IMDEA Materials Institute, Eric Kandel 2, Getafe, Madrid 28906 Spain.

http://dx.doi.org/10.1016/j.msea.2014.06.017
0921-5093/

the aim of this paper is the mechanical properties improvement of the Al–7 wt% Si alloy at intermediate-high temperatures by modifying its microstructure employing ECAP processing using route A, as well as the determination of the operating creep mechanisms.

2. Experimental procedure

The hypoeutectic Al–7 wt% Si alloy was prepared by melting appropriate proportions of pure aluminum (99.99 wt%) and eutectic Al–12.3 wt% Si master alloy and casting into an ingot 350 mm × 210 mm × 70 mm in size. A 0.02 wt% Na addition to the melt was employed in order to obtain a finer eutectic constituent. X-ray radiography was employed to assess porosity. The samples were machined from areas with the least apparent porosity.

ECAP billets, $90 \times 10 \times 10\ mm^3$, were machined from the as-cast ingot. ECAP processing was performed at room temperature using a sharp-cornered 90° ECAP die having die channels of square cross section. A schematic of the ECAP die used in this study is shown in Fig. 1. In this diagram, the plane where the simple shear occurs is located (marked with arrows) in the intersection of the two channels. FP, TP and CP denote the flow plane, top plane and cross plane after pressing respectively. Up to 8 repetitive ECAP passes were imposed using route A, which involves pressing without sample rotation between consecutive passes leading to a monotonically increasing strain.

The eutectic microconstituent distribution of the as-cast, 1p and 8p ECAP processed material was examined using an Olympus BH-2 optical microscope. For that purpose, the samples were ground and polished to a colloidal silica finish.

The (sub)grain size and small precipitates in the ECAP processed material were analyzed by means of a Zeiss Neon 40 field-emission scanning electron microscope (SEM) using the backscattered electron (BSE) signal. The samples were ground and polished to a colloidal silica finish and then electropolished using a solution consisting of 200 ml perchloric acid, 700 ml ethanol and 100 ml glycerol. Electropolishing was conducted at a potential of 15 VDC and temperature of −20 °C.

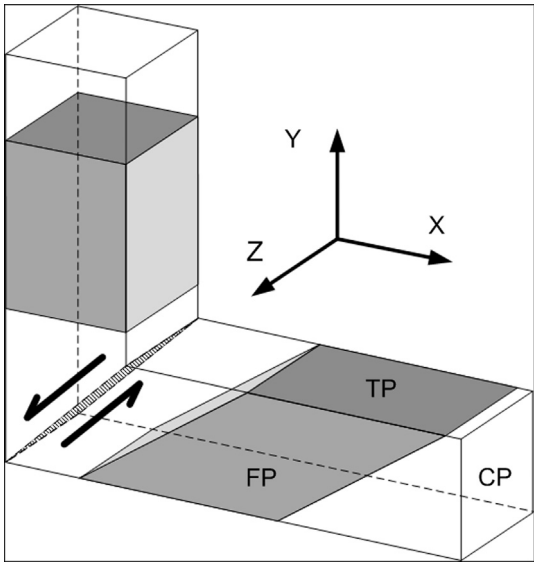

Fig. 1. Schematic illustration of an ECAP pass. The plane of the die channel intersection, where simple shear occurs as the billet passes through, is marked with arrows. FP, TP and CP denote the flow plane, top plane and cross plane after pressing respectively.

Grain size was measured on the primary Al constituent in the processed condition using BSE images. Scanning electron micrographs were analyzed using the Sigma Scan Pro software in order to obtain the size distribution of the aluminum matrix grains. The grains are not equiaxed in the processed alloy and so the minimum axis dimension of the grain was used as the grain size. More than 400 grains for each processing condition were analyzed. Size distribution histograms obtained from these measurements were conducted. Grain size data fell into lognormal distributions, so the geometric mean value was chosen as a measure of their size.

Planar dog-bone tensile samples with 6 mm × 2 mm × 1.8 mm gage dimensions were electro-discharge machined. The samples were machined parallel to the flow plane (FP), in such a way that the gage section coincided with the middle region of the ECAP samples avoiding frictional effects. Tensile samples were tested using a universal Instron 1362 testing machine equipped with a four-lamp ellipsoidal furnace to evaluate the mechanical behavior in the temperature range 200–400 °C. A set of tensile tests was performed at elevated temperatures and at constant cross-head speed of 0.065 mm s^{-1}, equivalent to an initial strain rate ($\dot{\varepsilon}$) of $10^{-2}\ s^{-1}$. Work of fracture values, U_T, were determined by computing the area under the σ vs ε curve. Additionally, another set was performed to determinate the apparent stress exponent, n_{ap}, and the apparent activation energy, Q_{ap}, using strain-rate-change (SRC) tests from 10^{-1} to $10^{-5}\ s^{-1}$. Limited ductility and the presence of porosity in the as-cast material made it difficult to perform SRC tests in this material, so a complementary set of tensile tests at constant strain rate of $10^{-4}\ s^{-1}$ was performed to determine the values of n_{ap} and Q_{ap}.

3. Results

3.1. Microstructure

Fig. 2a and b shows optical micrographs corresponding to the as-cast, hypoeutectic Al–7 wt% Si alloy. This microstructure consists on primary Al matrix dendrites surrounded by the eutectic constituent. The primary spherical-shaped Al dendrite cells are about 60–100 μm in size. Fig. 2b is a higher magnification image of eutectic constituent showing a distribution of irregularly shaped Si particles, about 5 μm in size (major axis).

It should be noted that a metastable super-saturated solid solution (~1.6 wt% Si) is retained in the aluminum matrix due to the relatively fast cooling rate following casting [17,18]. This super-saturated solid solution will help in the grain refining process during subsequent severe plastic deformation. The effects on the microstructure in the flow plane (FP) after one and eight ECAP passes by route A are shown in Fig. 3. Fig. 3a and b are optical micrographs showing the distribution of the primary Al matrix and eutectic constituents of the one ECAP pass (1p) and eight passes (8p) materials, respectively. After one pass the primary and eutectic constituents are elongated and inclined with respect to the axis of the die exit channel. Eight ECAP passes lead to a further elongation of both constituents and a lower inclination, reducing the separation between any two adjacent eutectic areas. A more detailed description can be found elsewhere [10,19]. SEM micrographs in Fig. 3c and d show eutectic Si particles after one and eight passes, respectively. The shear stress imposed on the plane defined by the intersection of the two channels into the ECAP die disrupts the 3-dimensional Si particles morphology in the eutectic structure. These particles are progressively refined and become smaller and more equiaxed with increasing number of passes (Fig. 3c and d) [18–20]. Fig. 3e and f present the (sub)grain structure in the Al primary matrix after one and eight passes,

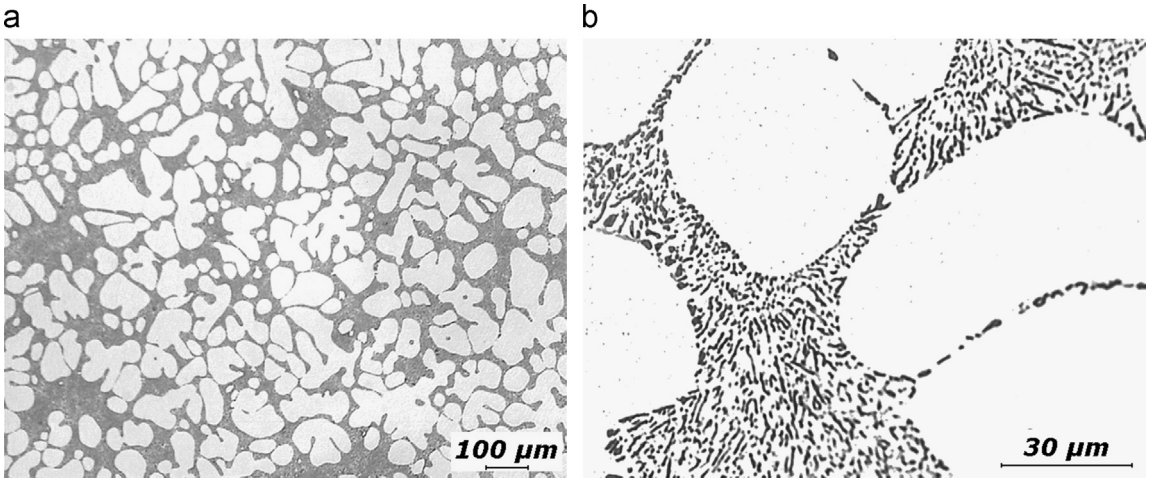

Fig. 2. Optical micrographs showing (a) as-cast dendritic microstructures of the Al–7 wt% Si alloy, and (b) a detail of the eutectic constituent morphology at higher magnification.

respectively, and illustrate grain refinement during processing. This is consistent with the observation that, after one ECAP pass, a substructure comprised of dislocation cells and subgrains having low-angle boundaries is formed (Fig. 3e), and, after eight passes, a similar microstructure is observed (Fig. 3f), although more recovered, with the presence of a higher fraction of high angle boundaries [19]. Fig. 3e and f also shows small precipitates (~50 nm) located on the (sub)grain boundaries in the Al matrix. These precipitates arise from the supersaturated solid solution of 1.6 wt% of Si in the primary Al constituent retained in the casting [17].

Fig. 4 illustrates the grain size distribution in the Al–7 wt% Si samples after one and eight ECAP passes. Grain size data fall into lognormal distributions, as usual in grain subdivision during deformation processing [21]. For the one ECAP pass (1p) sample the geometric mean grain size value is 250 nm, while for eight passes (8p) this value decreases to 210 nm. Additionally, the size distribution histogram for the 8p material has less data dispersion and is sharper than that for the 1p sample.

3.2. Mechanical properties

Fig. 5 shows plots of true stress vs true strain for samples tested in tension at different temperatures (200–400 °C) at constant cross-head speed of 0.065 mm s^{-1}, equivalent to an initial strain rate of 10^{-2} s^{-1}. Results for the as-cast Al–7 wt% Si alloy samples are plotted in Fig. 5a, whereas Fig. 5b and c correspond to the results for 1p and 8p materials, respectively.

Fig. 5a shows a decrease in the yield stress (σ_y) and maximum flow stress (σ_{max}) with an increase in test temperature for the as-cast material. The values of ductility (e_F) increase with increasing testing temperature. However, the eutectic structure, together with the porosity present in the as-cast material, results in low flow stress values and premature necking, thus giving limited work of fracture, U_T, and workability.

Both ECAP processed samples (Fig. 5b and c) show a similar trend with a stress decrease and ductility enhancement with increasing test temperature. However, the σ_y and σ_{max} values are much higher than for the as-cast material, especially at the lowest testing temperatures. Furthermore, the ductility of the processed materials is higher than that of the as-cast material at the highest testing temperatures. It is worth noting that the 1p material has a lower ductility than the as-cast material while the ductility of the 8p material is much larger at the lowest testing temperatures. This is attributed mainly to the microstructure comprised of dislocations and low angle boundaries for the 1p material, whereas the 8p material presents a more recovered microstructure.

Table 1 presents the work of fracture values for the as-cast, 1p and 8p materials as obtained from the area under the σ vs ε curves. Higher work of fracture values are obtained with increasing number of ECAP passes, especially at the lowest testing temperatures. Thus, the 8p material work of fracture is 5 times greater than that of the as-cast alloy at 200 °C.

In Fig. 6 the different mechanical behaviors at intermediate-high temperature of the as-cast Al–7 wt% Si alloy and the processed alloys through one and eight ECAP passes are compared. Fig. 6 shows the values of σ_y (Fig. 6a) and σ_{max} (Fig. 6b) vs temperature extracted from the curves in Fig. 5. The σ_y and σ_{max} values decrease for increasing testing temperature. Fig. 6a shows that both processed materials have higher values of σ_y than the as-cast material, especially at the lowest testing temperatures. The difference in σ_y values between processed and the as-cast materials decrease for increasing temperature in the temperature range 200–350 °C. Moreover, at $T \geq 350$ °C, the values are quite similar to those found for the as-cast material. The same trend is observed for the σ_{max} values in Fig. 6b.

The difference between σ_{max} and σ_y values for each temperature in Fig. 6 gives useful information about the strain-hardened state of the materials, and, therefore, of the processed microstructures. As expected, the highest values of $\sigma_{max} - \sigma_y$, up to 300 °C, correspond to both the as-cast material and the 8p material. The 1p material shows the lowest strain-hardening. This behavior is attributed to an already work-hardened microstructure comprised of dislocation tangles and low angle boundaries (subgrains) for the 1p material, in contrast to the more recovered (lower dislocation density) and more highly misoriented microstructure of the 8p material. The as-cast material consists of very coarse grains with absence of any work hardening. At $T \geq 350$ °C the strain-hardening behavior of the three materials is similar. At these temperatures the processed microstructures coarsen rapidly removing the dislocations and fine (sub)grains obtained by ECAP processing. The processed materials become microstructurally unstable and show similar mechanical properties to the as-cast material at high temperatures.

In order to determine the high temperature deformation behavior of the as-cast Al–7 wt% Si alloy, another set of tensile tests was performed at temperatures ranging 200–400 °C and at a constant cross-head speed of 6.5×10^{-4} mm s^{-1}, equivalent to an initial strain rate of 10^{-4} s^{-1}. In this way, two strain rate–flow stress data pairs were obtained for each testing temperature. The

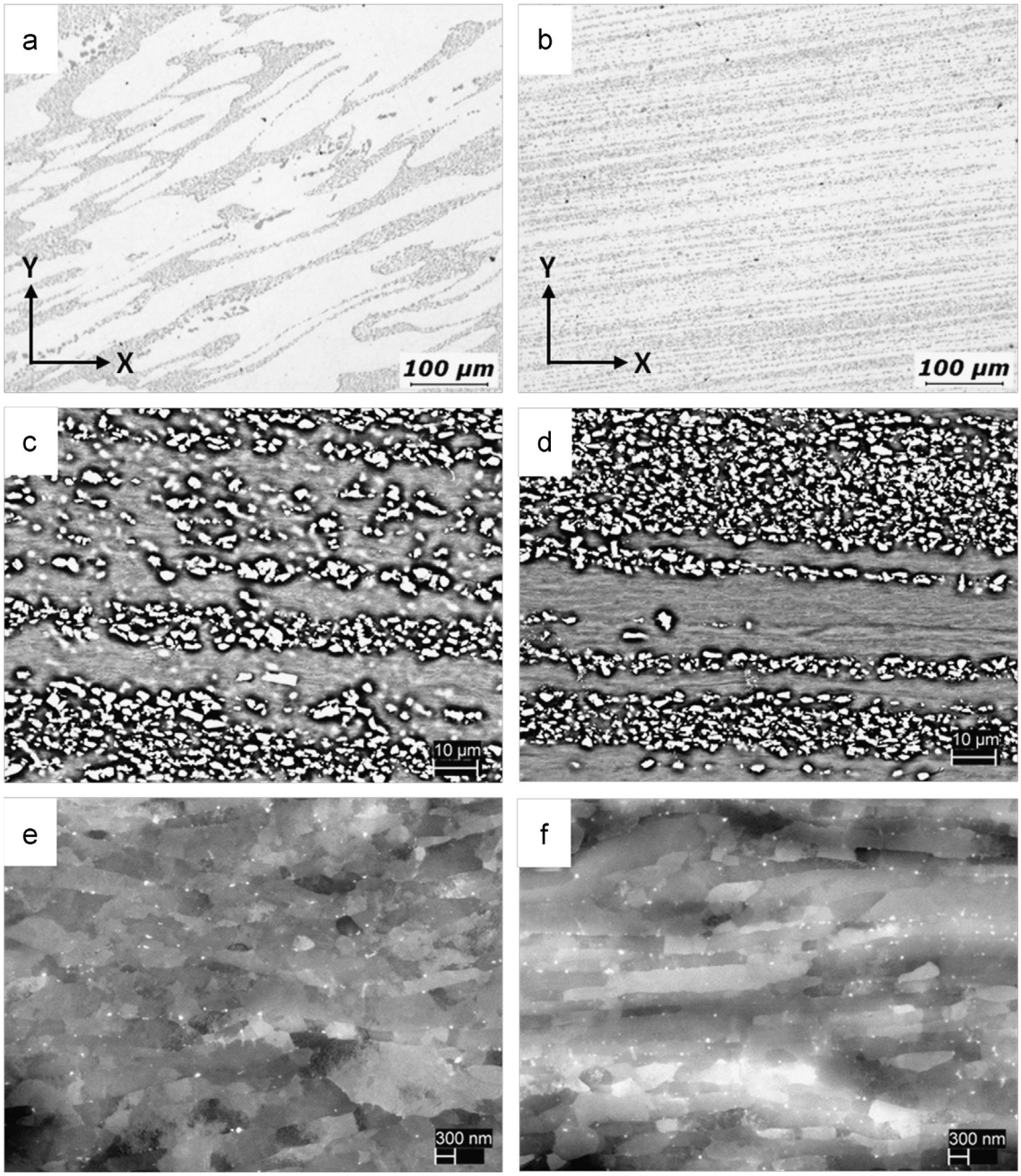

Fig. 3. Optical micrographs showing the evolution of microstructure and redistribution of the eutectic constituent in the FP of the Al–7 wt% Si alloy after (a) one ECAP pass and (b) eight ECAP passes using route A. SEM images showing eutectic Si particles size after (c) one ECAP pass and (d) eight ECAP passes, and at a higher magnification the presence of fine intradendritic Si precipitates and the grain size after (e) one ECAP pass and (f) eight ECAP passes following route A.

values of experimental or "apparent" stress exponent (n_{ap}) and apparent activation energy (Q_{ap}) are obtained using Eqs. (1) and (2) respectively, as follows:

$$n_{ap} = \frac{\Delta \log \dot{\varepsilon}}{\Delta \log \sigma}\bigg|_T \tag{1}$$

$$Q_{ap} = n_{ap} R \frac{\Delta \ln(\sigma/E)}{\Delta(1/T)}\bigg|_{\dot{\varepsilon}} \tag{2}$$

where T is the testing temperature and R is the gas constant. These values will aid in the assessment of the mechanism controlling deformation. The values of n_{ap} and Q_{ap} at each testing temperature for the as-cast alloy are presented in Table 2. The values of n_{ap} were obtained as the slope between the data at $10^{-2}\,s^{-1}$ and $10^{-4}\,s^{-1}$. High n_{ap} values are obtained, approaching $n_{ap} \approx 8$ as temperature increases, into the power law region. Q_{ap} values obtained at $10^{-2}\,s^{-1}$ present an average of 139 kJ/mol, close to 142 kJ/mol, which corresponds to the aluminum lattice self-diffusion (Q_L) value. These values of n_{ap} and Q_{ap} are in accordance with the operation of a constant substructure slip-creep mechanism.

The ECAP processed materials were much more ductile than the as-cast alloy so strain-rate-change (SRC) tests could be performed at different temperatures (200–400 °C) to obtain the values of n_{ap} and Q_{ap}. Strain rate–flow stress pairs ($\dot{\varepsilon}-\sigma$) were obtained once the steady state was reached for each strain rate change as detailed elsewhere [22]. During each change in $\dot{\varepsilon}$, after a small deformation, a new steady state was quickly developed, which is typical of the constant substructure deformation behavior [23].

The $\dot{\varepsilon}-\sigma$ data pairs at each testing temperature for the 1p and 8p materials are plotted in Fig. 7a and b respectively. In general,

stress values decrease for increasing temperatures and decreasing strain rates. The slope of each testing temperature curve, i.e., the n_{ap} value, decreases at the lower values of strain rate and this decrease is more noticeable at the higher temperatures. This is usually related to the occurrence of microstructural changes at high temperatures and long testing times.

Table 3 compiles the n_{ap} and Q_{ap} values evaluated at $\dot{\varepsilon}=10^{-2}\,s^{-1}$ and $10^{-4}\,s^{-1}$ at each testing temperature. At both strain rates the values of n_{ap} decrease with increasing testing temperature, as occurs in the as-cast material. At $\dot{\varepsilon}=10^{-2}\,s^{-1}$ n_{ap} tends to a value of up to 8, while at $\dot{\varepsilon}=10^{-4}\,s^{-1}$ n_{ap} decreases toward lower values. The values of Q_{ap} for the processed materials are, in general, somewhat higher than for the as-cast material. These variations in n_{ap} and Q_{ap} from the theoretical $n=8$ and $Q_L=142$ kJ/mol corresponding to the operation of a constant substructure slip-creep mechanism will be considered in Section 4.

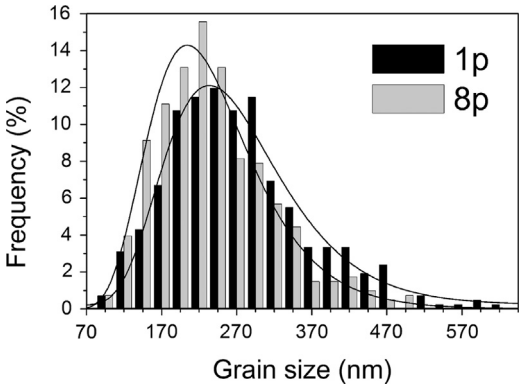

Fig. 4. (Sub)grain size distribution histogram determined by measuring more than 400 grains after one and eight ECAP passes.

4. Discussion

4.1. Microstructure

The heterogeneous as-cast hypoeutectic microstructure of the Al–7 wt% Si alloy (Fig. 2) was beneficially modified through ECAP processing by removing porosity, redistributing the eutectic constituent and refining the silicon particles (Fig. 2a–d). Although ECAP route A does not achieve a complete redistribution as it is obtained with FSP [24,25] and HPT [26,27], the mechanical properties are considerably improved with respect to the as-cast alloy. Additionally, from the first ECAP pass a fine (sub)grain microstructure, ~250 nm, is formed. Further ECAP passes, up to eight, achieve a slight decrease in the mean grain size, ~210 nm, with a more homogeneous grain size distribution, as shown in

Table 1
Work of fracture values for the as-cast, 1p and 8p Al–7 wt% Si alloy obtained as the area under the σ vs ε curves.

T (°C)	U_T, (MPa)		
	As-cast	ECAP 1p	ECAP 8p
200	9	8	43
250	13	15	27
300	14	12	20
350	6	14	18
400	9	14	11

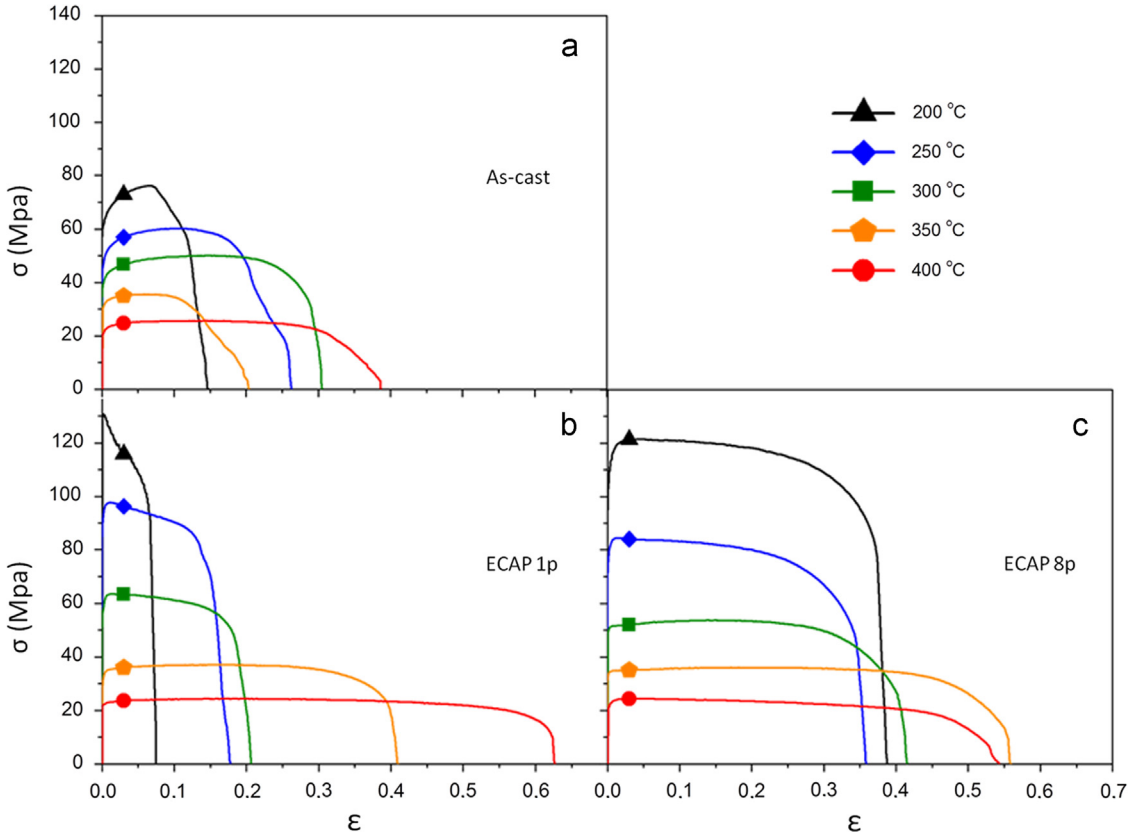

Fig. 5. True stress–true strain curves obtained from the tensile test at different temperatures and at a initial strain rate of $10^{-2}\,s^{-1}$ for (a) the as-cast, (b) 1p and (c) 8p material.

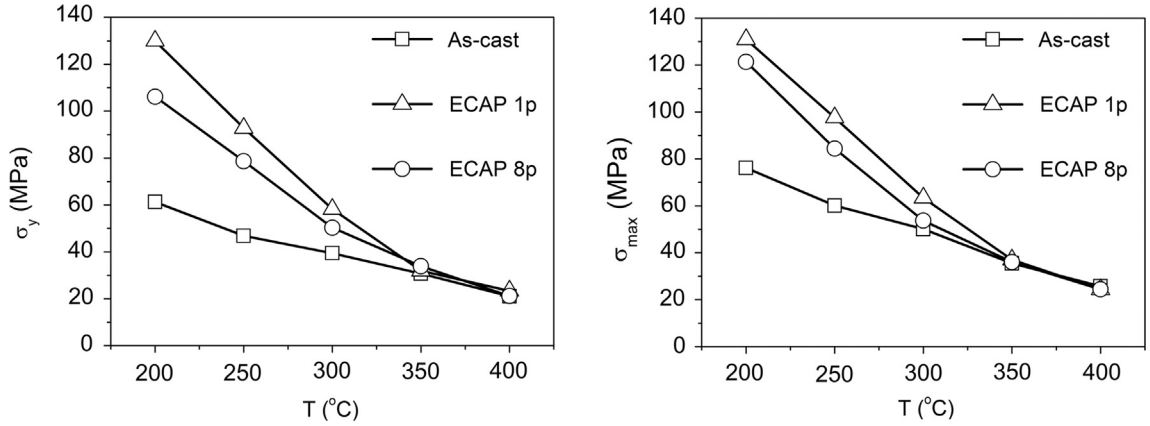

Fig. 6. Values of (a) σ_y (MPa) vs testing temperature (°C) and (b) σ_{max} (MPa) vs testing temperature (°C) for the as-cast Al–7 wt% Si alloy and for this alloy processed one and 8 ECAP passes.

Table 2
Values of n_{ap} and Q_{ap} at each testing temperature for the as-cast Al–7 wt% Si alloy.

T_e (°C)	n_{ap}	Q_{ap} (kJ/mol)
200	16.9	143
250	11.2	87
300	10.5	125
350	9.8	185
400	7.8	151
		$\langle Q_{ap} \rangle = 139$

Fig. 3. Those data indicate that the greater part of refinement is achieved from the first ECAP pass and further passes provide increasing recovery, grain boundary misorientation, and homogenization of grain size [19].

Previous studies demonstrated that the as-cast Al–7 wt% Si alloy retains about ~1.6 wt% Si in supersaturated solid solution within the aluminum matrix during air cooling after casting [17,18]. The subsequent deformation imposed upon the material during the ECAP processing causes strain-induced precipitation from the supersaturated solid solution in the form of homogeneously distributed fine Si precipitates (~50 nm) in the aluminum matrix. The presence of this fine precipitates aid the formation of a fine microstructure as shown in Fig. 3e and f. A considerable volume fraction of Si precipitates is obtained during the first ECAP pass, which is supported by the small variation of the (sub)grain size in further passes, as shown in the grain size distributions of Fig. 4, (250 nm after 1p vs 210 nm after 8p). The evolution of these fine Si precipitates will be important for the determination of the mechanical properties behavior at different temperatures. Fig. 8 shows a schematic diagram of the microstructural changes occurring during processing and testing of the alloy.

In this way, after one ECAP pass there are fine, intradendritic Si precipitates that retard dislocation movement. In addition, there is still some Si in solid solution which can precipitate both after further ECAP passes and during tensile testing at high temperature. In the case of the 8p material, precipitation is completed during processing, remaining the equilibrium concentration in the Al matrix (~0.05 wt% Si at room temperature). Therefore, precipitates only coarsen by the effect of temperature and strain during tensile testing [28].

4.2. Mechanical properties

The tensile tests in Fig. 5a show both the low strength and relatively poor ductility of the as-cast alloy in the temperature range investigated. This reflects the coarse primary–eutectic structure, a relatively brittle eutectic constituent and the presence of residual porosity. The mechanical behavior of the Al–7 wt% Si alloy was enhanced by ECAP processing as shown in Fig. 5b for one pass and in Fig. 5c for 8 ECAP passes. The strength increases from the first pass while ductility improvement requires more than one ECAP pass. This is attributed to a very high dislocation density together with the formation of low angle boundaries (subgrains) after one pass, while, for successive passes, the microstructure recovers progressively diminishing the dislocation density and increasing the amount of high angle boundaries as for the 8p material. In this regard, the values of work of fracture are higher in the processed material than in the as-cast alloy and increase with the number of ECAP passes, up to 5 times for the 8p sample at 200 °C. Thus, the ECAP processed Al–7 wt% Si alloy could be a candidate for more demanding applications.

The values of σ_y and σ_{max} as a function of temperature (Fig. 6a and b) give useful information regarding the microstructure evolution of the processed materials, which is greatly influenced by the evolution of the fine Si precipitation from the super saturated solid solution. The fine Si precipitates help in developing a fine substructure during room temperature ECAP processing when compared to such an alloy after long thermal treatments [17,18,29], and give higher strength as well as additional thermal stability at high temperatures as long as these precipitates can hinder (sub)grain growth. In this regard, according to the scheme of Fig. 8, the 1p material possesses a lower volume fraction of Si precipitates but which are also finer than those of the 8p material. Therefore, the 1p material will experience additional precipitation as a function of time and temperature, while precipitate coarsening occurs from the beginning of testing in the 8p material. Therefore, the 1p material is expected to show better stability in (sub)grain size values during high temperature tensile testing than the 8p material. This is corroborated in Fig. 6b, where the yield values for the 8p material tend to those found in the as-cast alloy at about 300 °C, while for the one ECAP pass 350 °C is needed.

4.3. Deformation mechanisms

Turning attention to the determination of the operating deformation mechanism, three possible mechanisms should be considered for this Al–7 wt% Si alloy – (i) slip-creep with stress-dependent subgrain formation ($n=5$), (ii) constant substructure slip-creep ($n=8$), and (iii) grain boundary sliding (GBS, $n=2$).

In the majority of pure metals and alloys with relatively coarse microstructures slip-creep is controlled by the climb of dislocations which self-organize to form a subgrain size (λ_{sg}) that is an

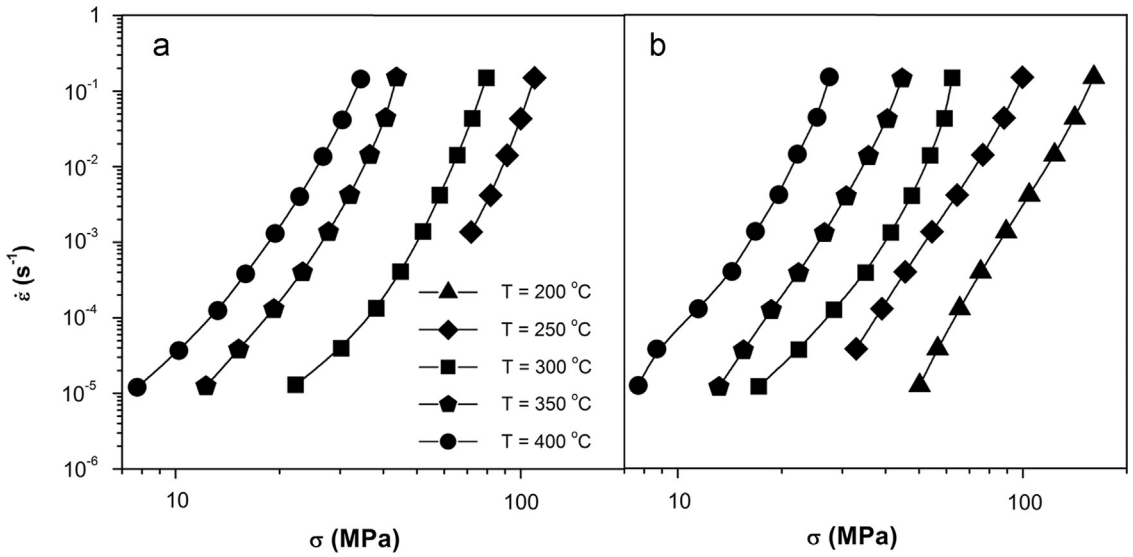

Fig. 7. $\dot{\varepsilon}-\sigma$ data pairs for the (a) 1p and (b) 8p material at different testing temperatures.

Table 3
Values of n_{ap} and Q_{ap} obtained at $10^{-2}\,s^{-1}$ and $10^{-4}\,s^{-1}$ at each testing temperature for the 1p and 8p materials.

Material	T_e (°C)	$n_{ap}^{10^{-2}}$	$n_{ap}^{10^{-4}}$	$Q_{ap}^{10^{-2}}$ (kJ/mol)	$\langle Q_{ap}^{10^{-2}} \rangle$ (kJ/mol)	$Q_{ap}^{10^{-4}}$ (kJ/mol)	$\langle Q_{ap}^{10^{-4}} \rangle$ (kJ/mol)
1p	250	11.5	–	169	204	–	171
	300	10.7	5.9	241		223	
	350	9.7	5.5	253		172	
	400	8.2	5.2	151		118	
8p	200	7.7	8.2	141	186	164	139
	250	7.5	7.1	129		125	
	300	10.8	5.3	199		94	
	350	8.5	6.4	189		167	
	400	9.2	4.7	270		144	

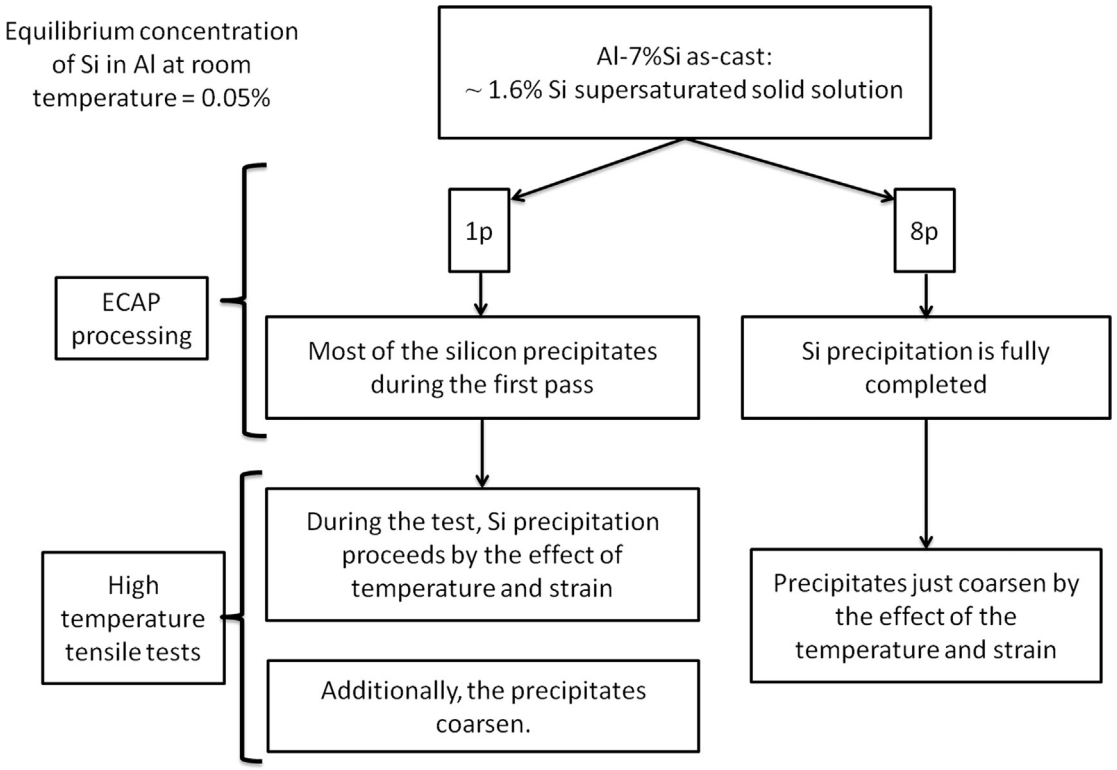

Fig. 8. Schematic diagram of the microstructural changes occurring during processing and testing of the alloy.

inverse function of the flow stress during deformation, as given by the following equation [23,30]:

$$\frac{\lambda_{sg}}{b} = K\frac{E}{\sigma} \tag{3}$$

where b is the Burgers vector, E is the Young modulus and K is ~8 in aluminum alloys [31]. The constitutive equation for the climb-controlled creep mechanism is the following [30]:

$$\dot{\varepsilon} = A\left(\frac{\sigma}{E}\right)^n \exp\left(-\frac{Q}{RT}\right) \tag{4}$$

where A is a constant, R is the gas constant, T is the test temperature, and, in the power-law region, $Q = Q_L$ is the activation energy for lattice self-diffusion, while the value of the stress exponent, n, is about 5. This mechanism does not operate in the present Al–7 wt% Si alloy due to Si in supersaturated solid solution in the as-cast condition as well as the presence of the fine precipitates (arising from the Si supersaturated solid solution) which lead to a substructure that is not a function of the stress as given by Eq. (3).

Another possible slip creep mechanism is that for which the formed (sub)grain size (λ_{sg}) is determined by the interparticle distance (λ_p), which in this case refers to the distance between the fine intradendritic precipitates coming from the supersaturated solid solution. This is because the distance between the fine Si precipitates is shorter than the interdendritic distance, delineated by the large eutectic Si particles. This substructure is determined by the particles/precipitates present, and is no longer dependent on the applied stress. This situation is referred to as "constant structure", "constant subgrain size", or "constant substructure", and its constitutive equation is the following [23]:

$$\dot{\varepsilon} = A\left(\frac{\lambda}{b}\right)^3 \left(\frac{\sigma}{E}\right)^n \exp\left(-\frac{Q_L}{RT}\right) \tag{5}$$

where λ is the smallest between λ_{sg} and λ_p, and the value of the stress exponent, n, is about 8.

A third mechanism, distinct from slip creep, is that wherein materials deform by grain boundary sliding (GBS) giving rise to superplastic deformation. This occurs in materials with microstructures consisting of stable, fine, equiaxed and highly misoriented grains. This high-temperature mechanism has an explicit dependence on the grain size (L) and very high elongations to failure are often obtained for optimal conditions of strain rate and temperature, together with very low flow stresses when compared to the conventional slip-creep stresses. The constitutive equation for this mechanism is [32]

$$\dot{\varepsilon} = A\left(\frac{b}{L}\right)^p \left(\frac{\sigma}{E}\right)^n \exp\left(-\frac{Q}{RT}\right) \tag{6}$$

where n is 2, and p is usually either 2 (if $Q = Q_L$) or 3 (if $Q = Q_{GB}$, the activation energy for self-diffusion along grain boundaries).

However, although very fine (sub)grains are obtained for the ECAP processes materials, no hint of superplastic deformation is observed from the results obtained (see Figs. 5–7). Elongations to failure are not high, stresses are much higher than for the pure Al and as-cast alloy, and stress exponents much higher than $n = 2$ are obtained. Thus it is possible that the heterogeneous primary–eutectic structure may redistribute the applied stress in a heterogeneous manner as well as hinder the accommodation of GBS. Furthermore, at high temperatures, the (sub)grains are not sufficiently stabilized by the fine Si precipitates, leading to excessive grain coarsening, and, at intermediate temperatures, the processed materials are not sufficiently equiaxed and highly misoriented to support superplastic behavior.

Therefore, the operating deformation mechanism in the Al–7 wt% Si materials should be constant substructure slip creep given by Eq. (5). In this case, the evolution of the fine Si precipitates will control the mechanical properties at high temperature, as discussed below.

A convenient way to compare the mechanical behavior between different materials is to normalize the $\dot{\varepsilon} - \sigma$ data with a diffusion coefficient and Young's modulus, respectively. Fig. 9a and b shows the mechanical behavior of 1p and 8p material respectively (colored filled symbols), compared with data from pure aluminum (open circles) [33] and the as-cast Al–7 wt% Si alloy (open squares). In these log–log-plots strain rate is normalized with the lattice self-diffusion coefficient (D_L) and the flow stress with Young's modulus (E) for each temperature [34]. It should be noted that compensation for all the materials was conducted using an activation energy of 142 kJ/mol, which corresponds to that for aluminum self-diffusion, in order to compare the behavior of the materials investigated here [35]. A horizontal dashed line represents power-law breakdown (PLB) at $\dot{\varepsilon}/D_L \approx 10^{13}$ m^{-2} indicating approximately the upper limit for the applicability of power law constitutive equations. Pure aluminum $\dot{\varepsilon}/D_L - \sigma/E$ data pairs below PLB are distributed along a line with a slope (n_{ap}) about 5. At values of $\dot{\varepsilon}/D_L \approx 10^{13}$ m^{-2} the values of n_{ap} increase rapidly. It is observed in the figure that the as-cast Al–7 wt% Si alloy is stronger than the pure aluminum in the temperature range investigated, and, additionally, the data exhibit higher values of n_{ap}, i.e. about 8 or higher, which is consistent with the operation of a slip-creep mechanism.

Fig. 9a shows that the Al–7 wt% Si alloy processed by just one ECAP pass is much more creep resistant than pure aluminum in the entire temperature range examined. The comparison of the mechanical behavior between the 1p material and the as-cast alloy shows that the processed material is more creep resistant than the as-cast material at $T \leq 300$ °C. At higher temperatures, the behavior of the ECAP processed material is similar to that of the as-cast alloy.

The mechanical behavior of the 8p material compared to both pure aluminum and the as-cast alloy is shown in Fig. 9b. As with the 1p material, the 8p material is more creep resistant than the pure aluminum in the entire temperature range studied. Also, the 8p material is more creep resistant than the as-cast alloy at 200 °C and at 250 °C at high $\dot{\varepsilon}$ values ($\dot{\varepsilon} \geq 3 \times 10^{-3}$ s^{-1}). At lower $\dot{\varepsilon}$ and higher temperatures the 8p material tends to be slightly less resistant than the as-cast material. Additionally, comparing both of the processed materials, one ECAP pass produces a stronger material than the 8p material, especially at $T \leq 300$ °C. These facts point again to microstructural changes, as will be discussed in the following.

A more in depth comparison of the processed materials in Fig. 9 reveals that while all the 8p material data fall on one curve, indicating monotonic behavior, the data for the 1p material show the following aspects: (i) higher creep resistance and greater slope at $T \leq 300$ °C, (ii) a curvature towards a smaller slope at 300 °C and low strain rates (long testing times), and (iii) a sudden strength drop at 350 °C towards similar values for the three materials. This convergence is supported by the increase of Si diffusivity with temperature that becomes important at 300 °C, and leads to coarsening of the fine precipitates and, thus, increasing the distance between them [28].

Based on these observations, and those from microstructural and mechanical characterization, the following general considerations on the high temperature deformation behavior of these materials can be made.

Unlike the pure aluminum, the as-cast Al–7 wt% Si has a supersaturated solid solution from which fine Si precipitates form during tensile testing as a function of temperature and strain.

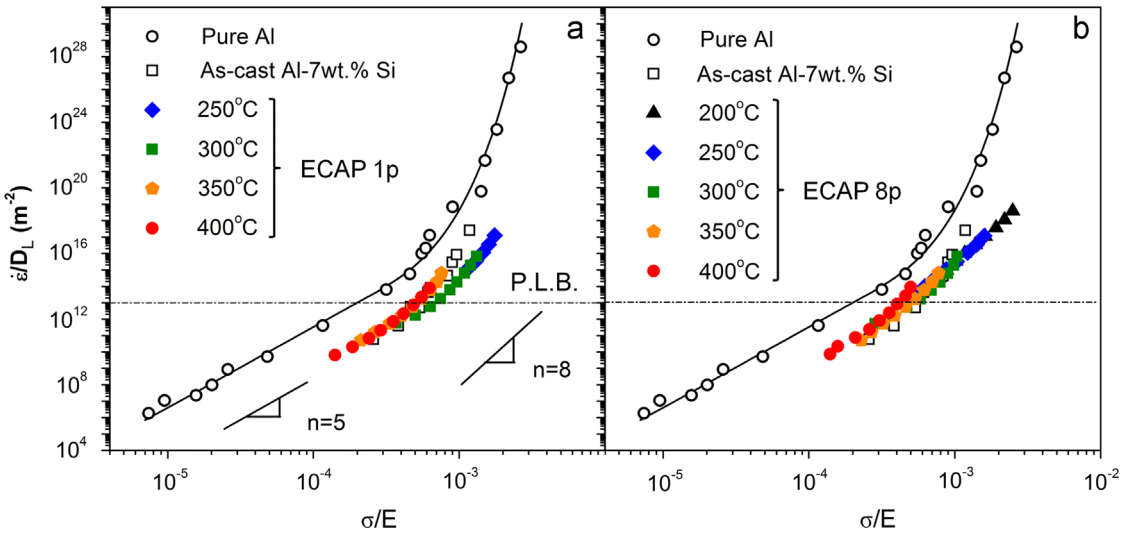

Fig. 9. $\dot{\varepsilon}/D_L - \sigma/E$ data pairs obtained from the strain rate changes tensile tests at different temperatures for (a) the 1p and (b) the 8p material and the as-cast alloy compared with data for pure aluminum [33].

Therefore, a finer substructure than that in pure Al is developed during the test, leading to the alloy becoming more creep resistant than the pure aluminum. This is consistent with the operation of a constant substructure slip-creep mechanism as described by Eq. (5).

In the case of the ECAP processed materials, as summarized in Fig. 8, the microstructure before testing consists of fine Al grains containing fine Si precipitates in the dendrite zones. In addition, for the 1p processed material, there is some Si in solid solution. As shown in Fig. 9, both processed materials are more creep resistant than the as-cast alloy and, basically, deformation is controlled by a constant substructure slip-creep mechanism with an associated $n=8$ as occurs in the as-cast alloy. The higher creep resistance of the processed materials is based on the smaller distance between the fine precipitates.

It is important to note that a "constant substructure" slip-creep mechanism with associated $n=8$ operates even with certain microstructural changes. This is general for any material where its "interparticle" distance (λ) remains smaller than the equilibrium stress-dependent subgrain size, predicted by Eq. (3). For the alloy studied, when the precipitates coarsen, n values lower than $n=8$ and Q values higher than $Q_L=142$ kJ/mol (Tables 2 and 3) are measured as well as decreasing slopes in the curves (Figs. 7 and 9). It must be borne in mind that Eq. (5) presents a λ^3 dependence, thus slight precipitate coarsening will have a noticeable effect in n_{ap} and Q_{ap} values.

The variations in n_{ap} and Q_{ap} values can be related analytically with the variations in λ during the tensile tests at high temperature [22,36,37]. In the power law region, when the constant substructure slip-creep mechanism is operative, the analytical relation for $n=n(\lambda)$ can be derived using its definition and Eq. (5) as follows:

$$n(\lambda)=\left.\frac{\partial \ln(\dot{\varepsilon})}{\partial \ln(\sigma/E)}\right|_T=\left.\frac{\partial \ln[(\sigma/E)^8(\lambda/b)^3]}{\partial \ln(\sigma/E)}\right|_T=\left.\frac{\partial \ln(\sigma/E)^8}{\partial \ln(\sigma/E)}\right|_T+\left.\frac{\partial \ln(\lambda/b)^3}{\partial \ln(\sigma/E)}\right|_T$$
$$=8+3\left.\frac{\partial \ln(\lambda)}{\partial \ln(\sigma)}\right|_T \quad (7)$$

In the same way, the analytical relation for $Q=Q(\lambda)$ can be derived using the definition of Q and Eq. (5)

$$Q(\lambda)=nR\left.\frac{\partial \ln(\sigma/E)}{\partial(1/T)}\right|_{\dot{\varepsilon}}=8R\left.\frac{\partial \ln(\dot{\varepsilon}/D_L)^{1/8}}{\partial(1/T)}\right|_{\dot{\varepsilon}}+8R\left.\frac{\partial \ln(\lambda/b)^{-3/8}}{\partial(1/T)}\right|_{\dot{\varepsilon}}$$
$$=Q_L-3R\left.\frac{\partial \ln(\lambda)}{\partial(1/T)}\right|_{\dot{\varepsilon}} \quad (8)$$

When the microstructure remains stable, $\Delta\lambda=0$, and $n=8$. Since the derivative of λ of Eq. (7) is negative, when the microstructure coarsens, $n<8$. Likewise, in the case of Q in Eq. (8), if the microstructure remains constant, $Q=Q_L$, but if it coarsens then $Q>Q_L$.

As $n_{ap}<8$ and $Q_{ap}>Q_L$ when $\Delta\lambda>0$, i.e. when the microstructure coarsens, the ratio Q_{ap}/n_{ap} will increase [37]. Fig. 10 shows the variation of Q_{ap}/n_{ap} with the temperature at two $\dot{\varepsilon}$ (10^{-2} and 10^{-4} s^{-1}) for the 8p material. The 8p material was selected to perform this analysis because all precipitation was completed before mechanical testing, as described in Fig. 8, and the present fine precipitates just grow gradually along deformation. The dashed line represents the theoretical value of $Q/n=Q_L/8=17.8$ kJ mol^{-1} K^{-1}. As it is observed in the figure, the values of Q_{ap}/n_{ap} for the processed alloy are close to $Q_L/8$ at $T\leq 300$ °C, which indicates that $\Delta\lambda\approx 0$. At $T>300$ °C, the ratio Q_{ap}/n_{ap} increases distinctly, indicating that λ increases with temperature due to the progressive coarsening of the fine precipitates in this temperature range.

In summary, ECAP has improved the as-cast Al–7 wt% Si alloy by refining the eutectic phase and the (sub)grain structure, and removing porosity which results in improving workability and work of fracture. The operative "constant substructure" slip creep mechanism renders the processed materials useful applications at temperatures up to 300 °C.

5. Conclusions

A Na-modified, as-cast Al–7 wt% Si alloy was subjected to repetitive equal channel angular pressing (ECAP) at ambient temperature using a 90° die and following route A, which involves monotonically increasing strain, up to 8 passes. Microstructural and mechanical characterization by tensile testing at high temperatures was performed. The following conclusions may be drawn:

1. The as-cast hypoeutectic microstructure, which includes a supersaturated Si solid solution (~1.6 wt% Si), is completely transformed by ECAP processing. From the first pass, porosity is removed, the eutectic constituent is broken up, the eutectic silicon particles are partially redistributed, and a fine and homogeneous silicon strain-induced-precipitation from the

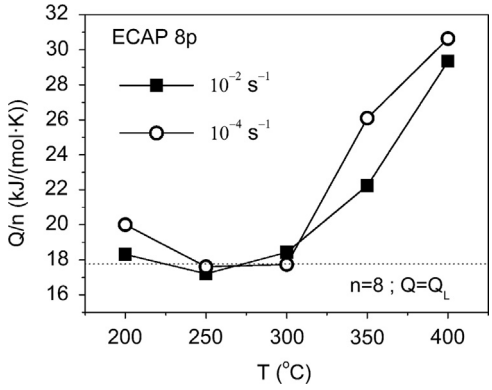

Fig. 10. Relation Q_{ap}/n_{ap} vs T for the 8p material at $10^{-2}\,s^{-1}$ represented by filled squares and $10^{-4}\,s^{-1}$ by open circles. The dashed line represents the theoretical value of $Q/n=Q_L/8$ for the constant substructure slip-creep mechanism.

supersaturated solid solution takes place. These fine precipitates assist in the grain refinement process, achieving (sub) grains about 250 nm after one pass and 210 nm after 8 passes.

2. The ECAP process is beneficial by increasing ductility and strength of the alloy, thus providing improved workability and work of fracture. After 8 ECAP passes by route A, the work of fracture is increased 5 times at 200 °C respect to the as-cast material. Therefore, the applicability of the Al–7 wt% Si alloy is expanded.
3. The material after one ECAP pass is more creep resistant than that after eight passes up to 300 °C. This is related to its more work-hardened microstructure comprised of dislocations, low angle boundaries and fine Si precipitates, which hinder dislocation movement during tensile testing. The 8p material is also more creep resistant than the as-cast material up to 300 °C due to the homogeneous distribution of fine Si precipitates resulting from processing.
4. The creep behavior of the three studied materials is controlled by the presence of the fine Si precipitates. The interparticle distance is too small to develop a stress-dependent subgrain size. Therefore, the constant substructure slip-creep mechanism controls deformation for all studied materials, with associated $n=8$ and $Q_L=142$ kJ/mol, as observed experimentally. Additionally, coarsening of these precipitates with time, temperature and strain induces increasing interparticle distances and variations in n_{ap} and Q_{ap} values, which are analytically predicted.

Acknowledgments

The financial support from Ministerio de Economía y Competitividad, Project MAT2012-38962, is gratefully acknowledged. A. Orozco-Caballero also thanks Consejo Superior de Investigaciones Científicas (Fellowship code: JAEPre_2010) for a JAE-Pre fellowship, co-funded by the European Social Fund (FSE 2007-2013). The authors also thank Dr. Jeffrey Woertz for his assistance in metallographic preparation at the Naval Postgraduate School.

References

[1] J.G. Kaufman, E.L. Roy, Aluminum Casting Alloys: Properties, Processes and Applications, American Foundry Society, ASM International, Materials Park, OH, 2004.
[2] C.M. Dinnis, A.K. Dahle, J.A. Taylor, Mater. Sci. Eng. A 392 (2005) 440–448.
[3] Y.C. Lee, A.K. Dahle, D.H. St.John, J.E.C. Hutt, Mater. Sci. Eng. A 259 (1999) 43–52.
[4] P.R. Goulart, J.E. Spinelli, W.R. Osorio, A. Garcia, Mater. Sci. Eng. A 421 (2006) 245–253.
[5] S. Khan, A. Ourdjini, Q.S. Hamed, M.A. Alam Najafabadi, R. Elliott, J. Mater. Sci. 28 (1993) 5957–5962.
[6] M.F. Hafiz, T. Kobayashi, Scr. Metall. Mater. 30 (1994) 475–480.
[7] C.H. Cáceres, C.J. Davidson, J.R. Griffiths, Mater. Sci. Eng. A 197 (1995) 171–179.
[8] Y. Estrin, A. Vinogradov, Acta Mater. 61 (2013) 782–817.
[9] H. Shi, D. Lu, H. Gong, R. Zhou, Adv. Mater. Res 472–475 (2012) 323–327.
[10] J.M. García-Infanta, A.P. Zhilyaev, C.M. Cepeda-Jiménez, O.A. Ruano, F. Carreño, Scr. Mater. 58 (2008) 138–141.
[11] Z.Y. Ma, S.R. Sharma, R.S. Mishra, Mater. Sci. Eng. A 433 (2006) 269–278.
[12] R.Z. Valiev, T.G. Langdon, Prog. Mater. Sci. 51 (2006) 881–981.
[13] V. Sklenička, J. Dvořák, M. Svoboda, Mater. Sci. Eng. A 387–389 (2004) 696–701.
[14] M. Kawasaki, I.J. Beyerleinb, S.C. Vogel, T.G. Langdon, Acta Mater. 56 (2008) 2307–2317.
[15] A. Orozco-Caballero, C.M. Cepeda-Jiménez, P. Hidalgo-Manrique, P. Rey, D. Gesto, D. Verdera, O.A. Ruano, F. Carreño, Mater. Chem. Phys. 142 (2013) 182–185.
[16] S. Sabbaghianrad, T.G. Langdon, Mater. Sci. Eng. A 596 (2014) 52–58.
[17] J.M. García-Infanta, S. Swaminathan, C.M. Cepeda-Jiménez, T.R. McNelley, O.A. Ruano, F. Carreño, J. Alloys Compd. 478 (2009) 139–143.
[18] C.M. Cepeda-Jiménez, J.M. García-Infanta, A.P. Zhilyaev, O.A. Ruano, F. Carreño, Mater. Sci. Eng. A 528 (2011) 7938–7947.
[19] J.M. García-Infanta, S. Swaminathan, A.P. Zhilyaev, F. Carreño, O.A. Ruano, T.R. McNelley, Mater. Sci. Eng. A 485 (2008) 160–175.
[20] A. Ma, K. Suzuki, Y. Nishida, N. Saito, I. Shigematsu, M. Takagi, H. Iwata, A. Watazu, T. Imura, Acta Mater. 53 (2005) 211–220.
[21] F.N. Rhines, Rev. Metal Madrid 22 (1986) 3–35.
[22] F. Carreño, O.A. Ruano, Acta Mater. 46 (1998) 159–167.
[23] O.D. Sherby, R.H. Klundt, A.K. Miller, Metall. Trans. A 8 (1977) 843–850.
[24] T.R. McNelley, E.S. Menon, Mater. Sci. Forum 706–709 (2012) 194–201.
[25] J.M. García-Infanta, A.P. Zhilyaev, F. Carreño, O.A. Ruano, J.Q. Su, S.K. Menon, T.R. McNelley, J. Mater. Sci. 45 (2010) 4613–4620.
[26] T. Mungole, N. Nadammal, K. Dawra, P. Kumar, M. Kawasaki, T.G. Langdon, J. Mater. Sci. 48 (2013) 4671–4680.
[27] C.M. Cepeda-Jiménez, A. Orozco-Caballero, J.M. García-Infanta, A.P. Zhilyaev, O.A. Ruano, F. Carreño, Mater. Sci. Eng. A 597 (2014) 102–110.
[28] Y. Birol, J. Alloys Compd. 439 (2007) 81–86.
[29] C.M. Cepeda-Jiménez, J.M. García-Infanta, A.P. Zhilyaev, O.A. Ruano, F. Carreño, J. Alloys Compd. 509 (2011) 636–643.
[30] O.D. Sherby, P.M. Burke, Prog. Mater. Sci. 13 (1968) 325–390.
[31] S.V. Raj, G.M. Pharr, Mater. Sci. Eng. 81 (1986) 217–237.
[32] O.A. Ruano, O.D. Sherby, Rev. Phys. Appl. 23 (1988) 625–637.
[33] D. Caillard, J.L. Martin, Rev. Phys. Appl. 22 (1987) 169–184.
[34] W. Köster, Z. Metallkd 39 (1948) 1–9.
[35] H.J. Frost, M.F. Ashby, Deformation-mechanism Maps: the Plasticity and Creep of Metals and Ceramics, Pergamon Press, 1982.
[36] F. Carreño, O.A. Ruano, Metall. Mater. Trans. A 30 (1999) 371–376.
[37] F. Carreño, O.A. Ruano, Rev. Metal. 37 (2001) 215–219.